# Full-field optical coherence tomography by achromatic phase shifting with a rotating polarizer

Yuuki Watanabe, Yasuhiro Hayasaka, Manabu Sato, and Naohiro Tanno

We demonstrate two-dimensional detection optical coherence tomography (OCT) using achromatic phase shifting with a rotating polarizer. This phase shifting, which experiences a light beam with a cyclic change in its polarization state, is, in principle, independent of wavelength. We simulated the wavelength dependence of an achromatic phase shifter using Jones calculus and found that the achromatic region exceeded 145 nm when the deviation of the phase retardation was less than $\pm 0.5°$. Using the achromatic phase shifter and a conventional phase-shift calculation method, we obtained *en face* OCT images of an onion at different depths. This method is effective to enhance the quality of OCT with an ultrabroad-spectrum light source. 

*OCIS codes:* 110.4500, 120.3180, 170.6900.

## 1. Introduction

Optical coherence tomography (OCT) is an emerging biomedical application that is capable of cross-sectional imaging of biological tissues with high spatial resolution ($\sim 10\ \mu m$) to depths of a few millimeters.[1–3] The axial resolution depends on the low coherence of the light source. Axial resolutions of 1–3 $\mu m$ have been demonstrated with an ultrabroad-spectrum light source.[4,5]

With full-field OCT methods we can measure *en face* images without $X$, $Y$ scanning using two-dimensional detection, such as with a CCD camera.[6,7] These methods have also been used to develop high-axial-resolution full-field OCT imaging with an ultrabroad-spectrum light source.[8,9] To obtain *en face* OCT images, a conventional phase-shifting technique that involves the shifting of the phase of the reference beam with a piezoelectric translator is often used. The subsequent processing is complicated by the fact that the phase shift introduced by changing the optical path is wavelength dependent. Therefore the conventional (monochromatic) phase-shifting calculation introduces systematic errors into the calculated results. A calculation algorithm that compensates for the phase errors has been proposed by use of a phase-shifting interferometer,[10] but since this algorithm needs five interference images, much time would be expended for the image acquisitions. Sinusoidal phase modulations have been used for full-field OCT imaging by a photoelastic modulator[7] and a piezoelectric translator.[8] However, these methods need four interference images and the optimizations of modulation parameters.

An alternative to phase shifting is to use the geometric phase (Pancharatnam phase).[11–17] This is the phase shift that is experienced by a light beam with a cyclic change in its state of polarization. The phase shift introduced by a polarizer is the same for all wavelengths. Therefore a sufficiently accurate calculation can be achieved with conventional phase-shifting algorithms such as three- or four-step phase-shifting methods. Such phase shifting has been demonstrated for surface profiling by use of white-light interferometry[11–13] and color digital holography.[16] However, these phase shifters use a rotating half-wave plate (HWP), placed between two quarter-wave plates (QWPs); achromatic phase shifting based on a rotating polarizer performs better.[14,15] Although the phase shifter with a rotating polarizer has been proposed by combinations of wave plates to obtain an achromatic phase shift, the wavelength dependence of the achromatic region has not been presented in detail. Furthermore, to our knowledge, the achromatic phase shifter has never been applied to obtain OCT images.

In this paper we report on full-field OCT imaging

The authors are with the Graduate School of Science and Engineering, Yamagata University, 4-3-16 Johnan, Yonezawa, Yamagata 992-8510, Japan. The e-mail address for Y. Watanabe is ywata@yz.yamagata-u.ac.jp.

Received 11 May 2004; revised manuscript received 22 October 2004; accepted 5 November 2004.

0003-6935/05/081387-06$15.00/0

with an achromatic phase shifter using a rotating polarizer. We calculated the wavelength dependence of the achromatic phase shifter using a Jones matrix and then compared a few combinations of wave plates for the light source used. The observed *en face* OCT images of an onion showed the structural differences at different depths.

### 2. Achromatic Phase Shifter with a Rotating Polarizer

We describe the principles of an achromatic phase shifter with a rotating polarizer.[14] Figure 1 shows the concept of the phase shifter with a rotating polarizer. The inputs are two orthogonal linearly polarized beams. Right-circularly polarized light is produced by passing linearly polarized light at an azimuth of 0° (horizontally polarized light) through a QWP whose fast axis is oriented at 45°. If the input light is polarized at an azimuth of 90° (vertically polarized light), then the output beam is left-circularly polarized. A rotating polarizer placed after the QWP acts as a phase shifter whose azimuth gives the phase of the output beam directly. When the input $\bar{E}_{\text{in}}$ is right-circularly polarized light, the Jones vectors for the light transmitted by the polarizer are given by

$$\begin{bmatrix} E_{R-x} \\ E_{R-y} \end{bmatrix} = P(\theta)\bar{E}_{\text{in}} = \begin{bmatrix} \cos^2\theta & \sin\theta\cos\theta \\ \sin\theta\cos\theta & \sin^2\theta \end{bmatrix} \begin{bmatrix} 1 \\ i \end{bmatrix} = \begin{bmatrix} \cos\theta \\ \sin\theta \end{bmatrix} \exp(i\theta), \tag{1}$$

where $E_{R-x}$ and $E_{R-y}$ are the $x$ and $y$ components of the transmitted light of the right-circularly polarized light. $P(\theta)$ is the Jones matrix of a polarizer at an azimuth of $\theta$. The output vectors of left-circularly polarized input light are also given by

$$\begin{bmatrix} E_{L-x} \\ E_{L-y} \end{bmatrix} = P(\theta)\bar{E}_{\text{in}} = \begin{bmatrix} \cos^2\theta & \sin\theta\cos\theta \\ \sin\theta\cos\theta & \sin^2\theta \end{bmatrix} \begin{bmatrix} 1 \\ -i \end{bmatrix} = \begin{bmatrix} \cos\theta \\ \sin\theta \end{bmatrix} \exp(i\theta), \tag{2}$$

where $E_{L-x}$ and $E_{L-y}$ are the $x$ and $y$ components of the transmitted light of the left-circularly polarized light. Rotating the polarizer by the angle $\theta$ results in one beam acquiring a phase shift of $\theta$ and the orthogonally polarized beam acquires a phase shift of $-\theta$. Thus the total phase difference introduced between two orthogonal linearly polarized beams is $2\theta$. The normal QWP introduces retardation of 90° at a mean wavelength. The QWP introduces retardation that varies with the wavelength. To obtain an achromatic circular polarizer, two configurations of wave plates have been proposed.[14] One combines a HWP at an azimuth of 15° and a QWP at an azimuth of 75°. The other combines a HWP at an azimuth of 6°, a HWP at an azimuth of 34°, and a QWP at an azimuth of 101°. The study of Ref. 14 demonstrated that the phase shifter produces only discrete values at three wavelengths.

First, we simulated the wavelength dependence of phase retardation for the above-mentioned configurations of the achromatic phase shifters using Jones calculus. For a horizontal linearly polarized input for a combination of a HWP and QWP, the output after the QWP is given by

$$\begin{bmatrix} E_x \\ E_y \end{bmatrix} = \mathrm{WP}(\delta_2,\ 75^\circ)\mathrm{WP}(\delta_1,\ 15^\circ) \begin{bmatrix} 1 \\ 0 \end{bmatrix}, \tag{3}$$

where $E_x$ and $E_y$ are the $x$ and $y$ components of the output beam after the QWP, respectively. $\delta_1$ and $\delta_2$ are the retardations of the HWP and QHP, respectively, at any wavelength. $\mathrm{WP}(\delta, \theta)$ is the Jones matrix of a wave plate at azimuth $\theta$ as follows:

$$\mathrm{WP}(\delta,\ \theta) = \begin{bmatrix} \cos(\delta/2) + j\sin(\delta/2)\cos 2\theta & j\sin(\delta/2)\sin 2\theta \\ j\sin(\delta/2)\sin 2\theta & \cos(\delta/2) - j\sin(\delta/2)\cos 2\theta \end{bmatrix}. \tag{4}$$

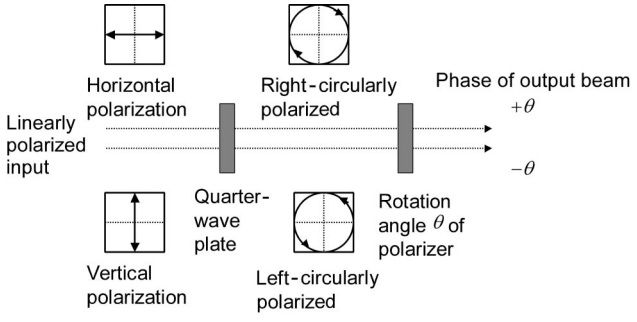


Fig. 1. Geometric phase shifter with a rotating polarizer.

The combination of two HWPs and a QWP is described by

$$\begin{bmatrix} E_x \\ E_y \end{bmatrix} = \mathrm{WP}(\delta_2,\ 101^\circ)\mathrm{WP}(\delta_1,\ 34^\circ)\mathrm{WP}(\delta_1,\ 6^\circ) \begin{bmatrix} 1 \\ 0 \end{bmatrix}. \tag{5}$$

Figure 2 shows the wavelength dependence of the phase retardation between $E_x$ and $E_y$. We also show the phase retardation of a QWP in Fig. 2. Here we assumed that the wave plates are designed with crystal quartz for a mean wavelength of 830 nm. The

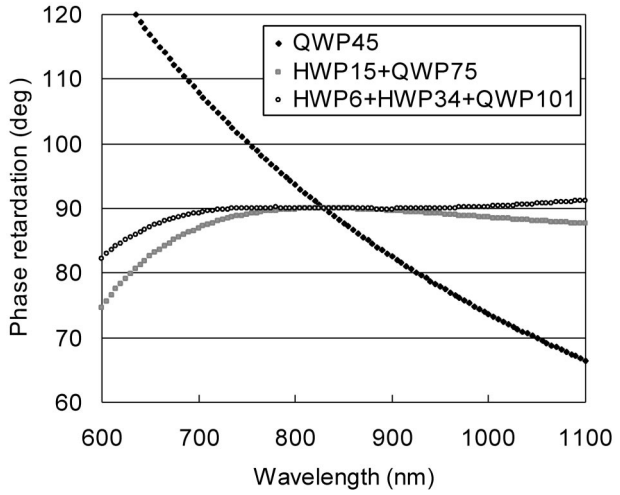


Fig. 2. Wavelength dependence of the phase retardation for three configurations. The wave plates were designed from crystal quartz for a mean wavelength of 830 nm.

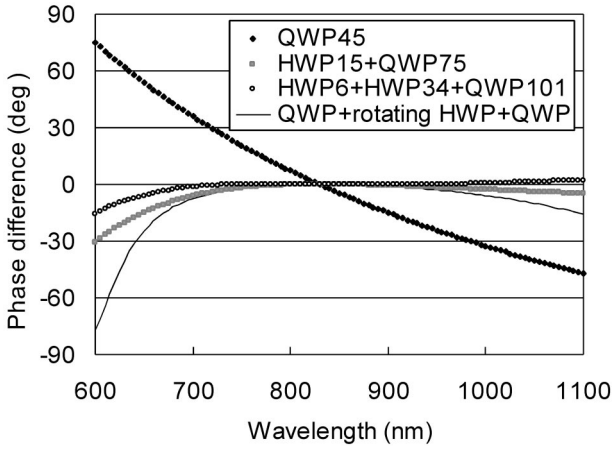


Fig. 3. Wavelength dependence of the phase difference at the three configurations. The solid curve is the phase difference of the rotating HWP achromatic phase shifter.

dispersion equation of crystal quartz uses the Laurent series formula that is described in the catalog of CVI Laser as follows:

$$n^2 = B_1 + B_2\lambda^2 + B_3/\lambda^3 + C_1/\lambda^4 + C_2/\lambda^6 + C_3/\lambda^8, \quad (6)$$

where the wavelength $\lambda$ is expressed in micrometers. The constants are $B_1 = 2.3849$, $B_2 = -1.259 \times 10^{-2}$, $B_3 = 1.079 \times 10^{-2}$, $C_1 = 1.6518 \times 10^{-4}$, $C_2 = -1.94741 \times 10^{-6}$, and $C_3 = 9.36476 \times 10^{-8}$ for an extraordinary ray and $B_1 = 2.35728$, $B_2 = -1.17 \times 10^{-2}$, $B_3 = 1.054 \times 10^{-2}$, $C_1 = 1.34143 \times 10^{-4}$, $C_2 = -4.45368 \times 10^{-7}$, and $C_3 = -5.92362 \times 10^{-8}$ for an ordinary ray. The combination of a HWP and QWP acts as a nearly achromatic circular polarizer. The combination of two HWPs and a QWP is a better achromatic circular polarizer. With both combinations, the achromatic region is broader in the wavelength region that is longer than the wavelength of 830 nm. When the deviation of the phase retardation is less than $\pm 0.5°$, we found that the single QWP, the configuration with one HWP and QWP, and the configuration with two HWPs and a QWP are 8, 145, and 330 nm, respectively. As both horizontally and vertically polarized lights are passed to the achromatic circular polarizer, the phase difference introduced between these lights has twice the wavelength dependence of the achromatic circular polarizer, as shown in Fig. 3. Here the phase difference at 830 nm is set to 0°. We also show the calculation for the alternative achromatic phase shifter that consists of a rotating HWP between two QWPs. From Fig. 3 we can see that achromatic phase shifting based on a rotating polarizer performs better than that based on a rotating HWP.

### 3. Experimental Setup

A schematic of our measurement system based on a Linnik interference microscope, i.e., a Michelson interferometer with identical objectives in both arms, is shown in Fig. 4. The light source is a superluminescent diode (SLD, Anritsu AS2C211, $P = 2$ mW), which has a central wavelength $\lambda_0 = 840$ nm and a $-3$-dB bandwidth $\Delta\lambda = 17$ nm. The resultant axial resolution is $\sim 18$ μm in air. The collimated output of the SLD is linearly polarized by the polarizer and then divided at the polarizing beam splitter into two orthogonally polarized beams. These beams pass through a QWP whose fast axis is oriented at 45° and are focused onto a reference mirror and a sample by use of two identical 10× microscope objectives with a numerical aperture of 0.25. The lateral resolution was $\sim 4$ μm when a test target was measured. QWPs are inserted into both arms to rotate the polarization by 90° on round trips in the interferometer. The beams are reflected at a reference mirror and a sam-

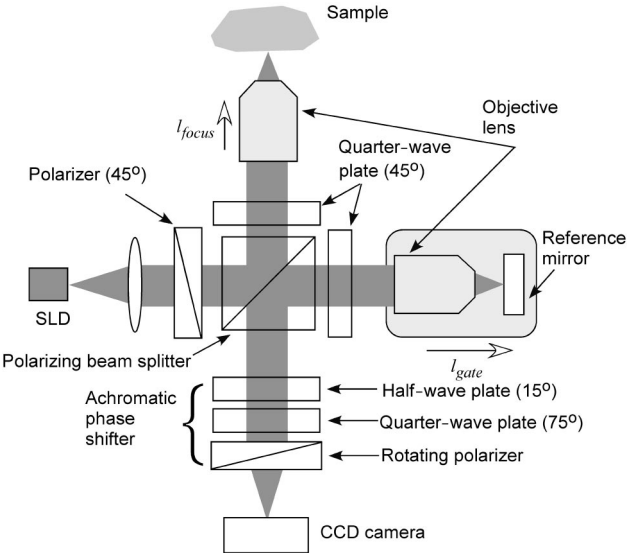


Fig. 4. Schematic of full-field optical coherence tomography by use of an achromatic phase shifter with a rotating polarizer. The achromatic phase shifter consists of a HWP at an azimuth of 15°, a QWP at an azimuth of 75°, and a rotating polarizer.

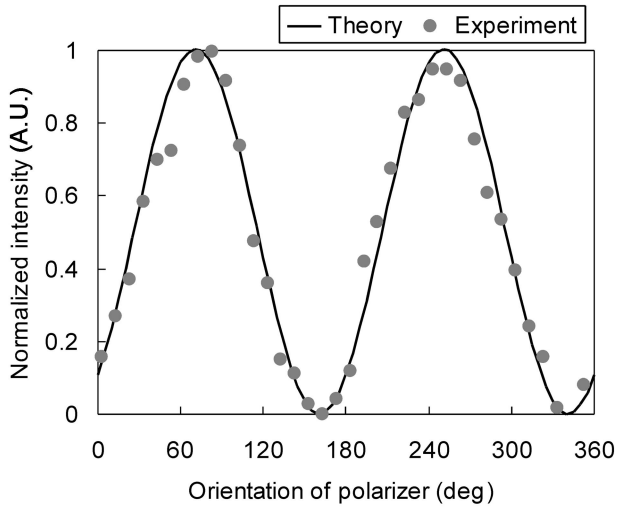


Fig. 5. Phase shifting with a rotating polarizer at various orientations from 0° to 360° at 10° intervals. The experimental data are the average values of nine pixels from the same region of each image. The solid curve is the theoretical values calculated with the Jones matrix.

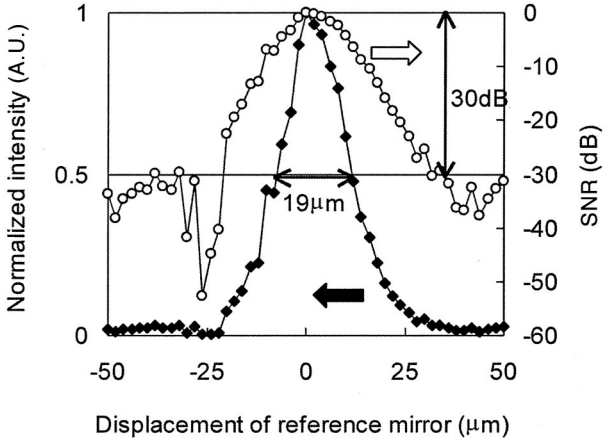


Fig. 6. Linear and logarithmic scales of an axial profile that were observed from interference components.

ple is passed to an achromatic phase shifter and then detected as an interference fringe with a CCD camera (Hamamatsu Photonics, C4880-81, pixels, 656 × 494; pixel size, 9.9 μm × 9.9 μm). The rotation of the polarizer, which is assembled on a stepper motor, is controlled with a personal computer by a general-purpose interface bus. We selected the combination of a HWP at an azimuth of 15° and a QWP at an azimuth of 75° to obtain enough achromatic phase shifts in the spectrum region of the SLD used. These wave plates were designed with crystal quartz for a mean wavelength of 830 nm.

To ensure phase shifting when rotating the polarizer, we measured the interference fringes using a mirror to sample at various orientations from 0° to 360° at 10° intervals. The normalized mean values of nine pixels in the same region of each image are shown in Fig. 5. The values agree with the values calculated with the Jones matrix. We can see that the phase shift is twice the rotation angle, as shown by Eqs. (1) and (2).

#### 4. *En Face* Optical Coherence Tomography Imaging

We used the conventional phase-shift algorithm to obtain an *en face* OCT image. The interference image $I_{2\theta}$, which occurs when the polarizer is rotated $\theta$, is as follows:

$$I_{2\theta} = I_S + I_R + 2\sqrt{I_S I_R}\cos(\phi + 2\theta), \tag{7}$$

where $I_S$ and $I_R$ are the intensities of the signal and reference beams, respectively, and $\phi$ is the initial phase difference. Additional phase differences of 0°, 120°, and 240° are introduced by rotating the polarizer 0°, 60°, and 120°, respectively. The observed interference component $I$ by the three-step phase-shift calculation is as follows:

$$I = 2\sqrt{I_S I_R} = [(2I_{120} - I_0 - I_{240})^2 + 3(I_0 - I_{240})^2]^{1/2}/3. \tag{8}$$

The rotation of the polarizer and the three-step phase-shift calculation expended 1.8 and 0.6 s/image, respectively.

First we estimated the axial resolution and the signal-to-noise ratio (SNR) of our imaging system. We measured the interference components by moving the reference mirror axially in steps of 2 μm. Here we inserted a neutral-density filter in the reference arm to reduce the intensity of the reference beam. Figure 6 shows the axial profile of the interference components that was obtained from a pixel value located at the same point in each image. The full width at half-maximum of the axial profile was 19 μm; this is close to the theoretical value of 18 μm. Although the measured axial resolution was degraded only 1 μm by the dispersion effect of the neutral-density filter, we do not need the dispersion compensation when imaging into scattering media when the SLD is used. It is necessary to image the dispersion compensation with a broader-spectrum light source. The axial profile is also plotted on a logarithmic scale in Fig. 6. The SNR of the axial profile was approximately 30 dB.

For imaging in the axial direction, both the coherence gate and the focal plane need to be adjusted. Consider the measurement of a layer sample with refractive index $n$ and geometric thickness $d$. First, the coherence gate and focal plane are positioned on the front surface of the sample. Next, the coherence gate is moved to the rear surface of the sample by moving the reference mirror $l_{\text{gate}} = nd$. The focal plane is also shifted to the rear surface of the sample by moving the objective lens $l_{\text{focus}} = d/n$ in the sample arm. Therefore the displacement relationship of the coherence gate and focal plane can be represented as $l_{\text{focus}} = l_{\text{gate}}/n^2$. We confirmed this relation experimentally. The imaging target consisted of two test pat-

terns [Fig. 7(a)]. The geometric thickness and refractive index were $d = 1.5$ mm and $n = 1.5$, respectively. First, the coherence gate and focal plane were positioned on the rear surface of the positive test pattern [Fig. 7(b)]. Then the coherence gate was shifted to the rear surface of the negative test pattern by moving the reference mirror to $l_{\mathrm{gate}} = 2454$ μm. The focal plane was aligned with the rear surface of the negative test pattern by moving the objective lens in the sample arm, as shown in Fig. 7(c). The displacement of the lens was 1089 μm, which was close to $l_{\mathrm{focus}} = l_{\mathrm{gate}}/n^2 = 1090$ μm. We confirmed that the displacements of the coherence gate and focal plane satisfied the above-mentioned relation.

Finally, we describe tomographic images of scattering media. We measured *en face* OCT images of an onion from the surface to a 200-μm scan depth by adjusting the reference mirror and objective lens. Here we assumed that the mean refractive index of an onion is 1.4. Figure 8(a) shows a microscopic image of an onion surface as reference. This image is 486 μm × 400 μm in size. As an example, Fig. 8(b) shows an interference fringe from the onion surface. Since the reflected light is strong at the surface because of the refractive-index mismatch between air and the sample, the interference fringes are clearly visible. The image size is 304 μm × 229 μm. The interference fringe from the inside of the scattering media is weak because the intensity of the surface reflection dominates in the interference image as noninterference components. Figures 8(c)–8(e) show *en face* OCT images of an onion at 0 (surface), 100, and 200 μm, respectively. To visualize the weak interference components clearly, these images are presented in logarithmic scale. We can see the cell structures of the onion at different depths and the structural differences in these images.

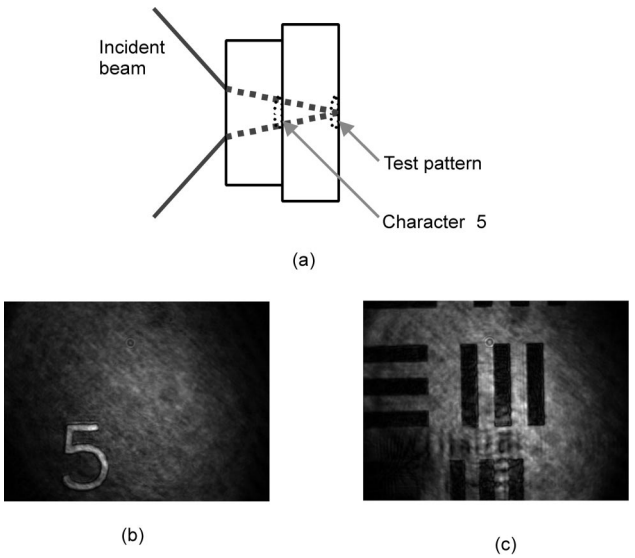


Fig. 7. (a) Schematic of an imaging target consisting of two test patterns. (b) Coherence gate and focal plane were positioned on the rear surface of the positive test pattern. (c) Coherence gate and focal plane were positioned on the rear surface of the negative test pattern.

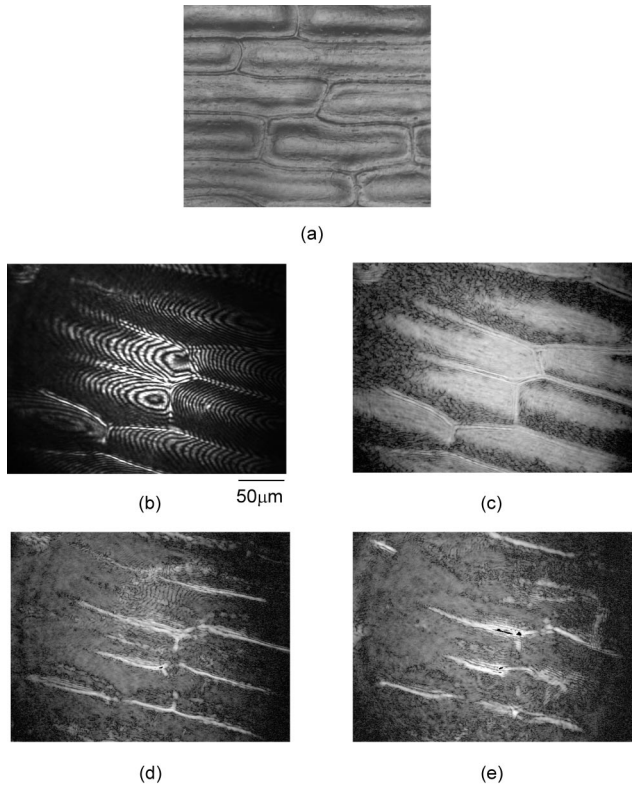


Fig. 8. (a) Microscopic image of an onion as reference. The image measures 486 μm × 400 μm. (b) Interference fringe at an onion surface. *En face* OCT images of an onion at different depths: (c) 0 (surface), (d) 100, and (e) 200 μm. The gray scale is logarithmic. The image size is 200 μm.

## 5. Discussion and Conclusion

We demonstrated axial direction imaging of full-field OCT using an achromatic phase shifter with a rotating polarizer. The achromatic phase shifter could be effective for imaging by use of a broader-spectrum light source. By simulating the wavelength dependences of the achromatic region, we found that the single QWP, the configuration with one HWP and QWP, and the configuration with two HWPs and a QWP are 8, 145, and 330 nm, respectively, when the deviation of the phase retardation is less than ±0.5°. We confirmed the phase shifting using a Linnik interference microscope with the achromatic phase shifter experimentally and then measured the *en face* OCT images of an onion at different depths. To obtain high-resolution sectioning of full-field OCT images with an ultrabroad-spectrum light source, such as a femtosecond Ti:sapphire laser or a tungsten–halogen lamp, the achromatic circular polarizer that we used must have a combination of two HWPs and a QWP, based on our Jones calculations. Note that dispersion compensation is important to use for the ultrabroad-spectrum light source.

If a sample has birefringence, the polarization state of the sample beam, which passes through a

QWP, is not linear. As the polarizing beam splitter selects the horizontally polarized light from the returned light, the effects of the birefringence would not appear in the resultant OCT images.

The SNR of the full-field OCT image depends on the fringe visibility of the interference signal, the full well capacity of a CCD camera, and the number of image accumulations.[7] The measured SNR of our system was approximately 30 dB without accumulation. The improvement of our SNR can be achieved by the image accumulations. We achieved the *en face* OCT images of an onion at a 200-μm scan depth. If we measure a deeper region by increasing incident power, the CCD camera saturates by the strong reflected light at the surface because of the refractive-index mismatch between air and the sample. Therefore use of a water immersion objective to reduce the surface reflection could increase the depth of penetration.

The measurement times depended on the speed of rotation of the polarizer. In general, once the rotation rate reaches a given speed, the speed remains constant. As the high-speed rotational stage is commercially available, the stable and continuous phase shifting introduced with high-speed polarizer rotation could realize real-time high-resolution full-field OCT imaging.

In conclusion, we have demonstrated full-field OCT using an achromatic phase shifter with a rotating polarizer. Since the phase shift introduced by a polarizer is the same for all wavelengths, conventional (monochromatic) phase-shifting algorithms can achieve a sufficiently accurate image. Using this phase shifter, we obtained *en face* OCT images of an onion from the surface to a 200-μm scan depth. The achromatic phase shifter could be effective for imaging with a broader-spectrum light source.

## References


1. D. Huang, E. A. Swanson, C. P. Lin, J. S. Schuman, W. G. Stinson, W. Chang, M. R. Hee, T. Flotte, K. Gregory, C. A. Puliafito, and J. G. Fujimoto, "Optical coherence tomography," Science **254,** 1178–1181 (1991).
2. J. A. Izatt, M. D. Kulkarni, H. W. Wang, K. Kobayashi, and M. V. Sivak, Jr., "Optical coherence tomography and microscopy in gastrointestinal tissues," IEEE J. Sel. Top. Quantum Electron. **2,** 1017–1028 (1996).
3. G. J. Tearney, M. E. Brezinski, B. E. Bouma, S. A. Boppart, C. Pitris, J. F. Southern, and J. G. Fujimoto, "*In vivo* endoscopic optical biopsy with optical coherence tomography," Science **276,** 2037–2039 (1997).
4. W. Drexler, U. Morgner, F. Kartner, C. Pitris, S. Boppart, X. Li, E. Ippen, and J. G. Fujimoto, "*In vivo* ultrahigh resolution optical coherence tomography," Opt. Lett. **24,** 1221–1223 (1999).
5. Y. Wang, Y. Zhao, J. S. Nelson, Z. Chen, and R. S. Windeler, "Ultrahigh-resolution optical coherence tomography by broadband continuum generation from a photonic crystal fiber," Opt. Lett. **28,** 182–184 (2003).
6. E. Beaurepaire, A. C. Boccara, M. Lebec, L. Blanchot, and H. Saint-Jalmes, "Full-field optical coherence microscopy," Opt. Lett. **23,** 244–246 (1998).
7. A. Dubois, L. Vabre, A. C. Boccara, and E. Beaurepaire, "High-resolution full-field optical coherence tomography with a Linnik microscope," Appl. Opt. **41,** 805–812 (2002).
8. L. Vabre, A. Dubois, and A. C. Boccara, "Thermal-light full-field optical coherence tomography," Opt. Lett. **27,** 530–532 (2002).
9. B. Laude, A. De Martino, B. Drevillon, L. Benattar, and L. Schwartz, "Full-field optical coherence tomography with thermal light," Appl. Opt. **41,** 6637–6645 (2002).
10. P. Hariharan, B. F. Oreb, and T. Eiju, "Digital phase-shifting interferometry: a simple error-compensating phase calculation algorithm," Appl. Opt. **26,** 2504–2506 (1987).
11. P. Hariharan and M. Roy, "White-light phase-stepping interferometry for surface profiling," J. Mod. Opt. **41,** 2197–2201 (1994).
12. P. Hariharan and M. Roy, "Achromatic phase-shifting for two-wavelength phase-stepping interferometry," Opt. Commun. **126,** 220–222 (1996).
13. S. S. Helen, M. P. Kothiyal, and R. S. Sirohi, "Achromatic phase shifting by a rotating polarizer," Opt. Commun. **154,** 249–254 (1998).
14. S. S. Helen, M. P. Kothiyal, and R. S. Sirohi, "Phase shifting by a rotating polarizer in white-light interferometry for surface profiling," J. Mod. Opt. **46,** 993–1001 (1999).
15. S. S. Helen, M. P. Kothiyal, and R. S. Sirohi, "White-light interferometry with polarization phase-shifter at the input of the interferometer," J. Mod. Opt. **47,** 1137–1145 (2000).
16. J. Kato, I. Yamaguchi, and T. Matsumura, "Multicolor digital holography with an achromatic phase shifter," Opt. Lett. **27,** 1403–1405 (2002).
17. M. Roy, P. Svahn, L. Cherel, and C. J. R. Sheppard, "Geometric phase-shifting for low-coherence interference microscopy," Opt. Laser Eng. **37,** 631–641 (2002).